JMEPEG (2006) 15:336-344
DOI: 10.1361/105994906X108648

1059-9495/$19.00

Cracking of Martensitic Alloy EP-823 Under Controlled Potential

A.K. Roy and M.K. Hossain

(Submitted March 28, 2005; in revised form November 15, 2005)

The susceptibility of martensitic Alloy EP-823 to stress corrosion cracking was evaluated with and without an applied cathodic potential using the slow-strain-rate (SSR) testing technique. The magnitude of the applied potential was based on the corrosion potential determined by cyclic polarization. The cracking susceptibility in an acidic environment at different temperatures was expressed in terms of the true failure stress (σ_f), time to failure (TTF), and ductility parameters, including percent elongation (%El) and percent reduction in area (%RA). The data indicate that the magnitudes of σ_f, TTF, %El, and %RA were reduced due to cathodic charging. The scanning electron microscopic evaluations of the primary fracture surface of the specimens used in SSR testing revealed a combination of ductile and brittle failures. Further, the secondary cracks at the gauge section of these specimens were characterized by branching.

Keywords Alloy EP-823, cathodic polarization, failure analyses, hydrogen-induced cracking

1. Introduction

Martensitic Alloy EP-823 has been identified as a target structural material for transmutation applications. Transmutation is a process of transforming long-lived isotopes to species with relatively short half-lives and reduced radioactivity through capture of minor actinides and fission products. Such reduction in half-life and radioactivity in high-level radioactive waste and spent nuclear fuel may enable their disposal for shorter durations in the proposed Yacca Mountain repository located near Las Vegas, NV.

During the transmutation process, a significant amount of hydrogen can be generated, which will promote environment-induced degradations such as stress corrosion cracking (SCC) and hydrogen-embrittlement (HE) of Alloy EP-823 (Ref 1, 2). This alloy was developed by the Russians for nuclear applications because of its superior corrosion resistance resulting from the presence of increased silicon (Si) content. In addition, this alloy possesses significant resistance to swelling during high neutron exposure at temperatures up to 420 °C, low rate of irradiation creep, and rather low activation compared to that of the austenitic stainless steels (Ref 3, 4). This alloy has also been reported to retain its high strength and ductility at elevated temperatures in irradiated conditions (Ref 5).

The structural materials including a martensitic Alloy EP-823 are known (Ref 6) to undergo environment-assisted crack-

A.K. Roy and **M.K. Hossain,** Department of Mechanical Engineering, University of Nevada, Las Vegas (UNLV), 4505 Maryland Parkway, Las Vegas, NV 89154-4027. Contact e-mail: aroy@unlv.nevada.edu.

Table 1 Chemical composition of Alloy EP-823 (wt.%)

Material/heat number	C	Mn	P	S	Si	Cr	Ni	Mo	Cu	V	W	Cb	B	Ce	Fe
EP-823/2055	0.16	0.57	0.014	0.004	1.14	11.71	0.67	0.74	0.002	0.31	0.58	0.23	0.009	0.04	Balance

Table 2 Composition (gram/liter) of test solution

Environment, pH	$CaCl_2$	K_2SO_4	$MgSO_4$	NaCl	$NaNO_3$	Na_2SO_4	HCl
Acidic, 2.35	2.769	7.577	4.951	39.973	31.529	56.742	Added to adjust the desired pH

Fig. 1 Specimen configurations: (a) smooth tensile specimen and (b) electrochemical polarization specimen

ing such as SCC due to the synergistic effect of applied and/or residual stress and a potent aqueous environment. Though these environments may vary, the structural stability of the protective oxide film on the material's surface may play a significant role in influencing the cracking susceptibility. There are indications in the open literature (Ref 7, 8) that hydrogen can be absorbed on the material's surface due to cathodic charging. The detrimental effect of hydrogen resulting from cathodic applied potential in enhancing hydrogen-induced embrittlement (HE) of susceptible materials has been reported by numerous investigators (Ref 9-12). This paper presents the results of SCC testing of Alloy EP-823 with and without the application of a cathodic potential. The results of localized corrosion testing and metallographic and fractographic evaluations of the tested specimens are also included.

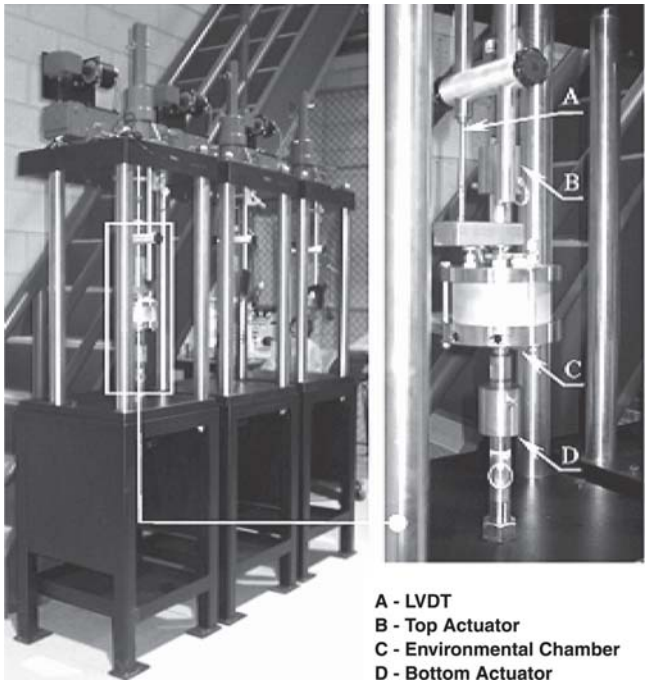

Fig. 2 Slow-strain-rate test setup

2. Material and Environment

An experimental heat of Alloy EP-823 was melted by a vacuum-induction-melting (VIM) practice. The chemical composition of this alloy is given in Table 1. The VIM ingot was then subjected to metallurgical processing that included forging and hot rolling into round bars of desired dimensions. This material was austenitized at 1850 °F (1010 °C) followed by an oil quench to produce hard but brittle martensite. Subsequently, it was tempered at 1150 °F (621 °C) for 1.75 h and air cooled to achieve a fine-grained and fully tempered-martensitic microstructure without the formation of any retained austenite.

Smooth cylindrical specimens (101.6 mm overall length, 25.4 mm gauge length, and 6.35 mm gauge diameter) were machined from the heat-treated round bars of this alloy in such a way that the gauge section was parallel to the longitudinal rolling direction. These cylindrical specimens were used in tensile properties and SCC evaluations of Alloy EP-823. For localized corrosion testing, smaller-sized cylindrical specimens having length and diameter of 12.7 and 9.398 mm, respectively, with a central blind hole for holding the specimen were used. The configurations of both types of test specimen are shown in Fig. 1. The test solution chemistry is given in Table 2.

Table 3 Hardness of Alloy EP-823 under different heat-treatment conditions

Heat-treatment condition	Hardness, R_c
Austenitized and quenched	41
Quenched and tempered for 1.75 h	26

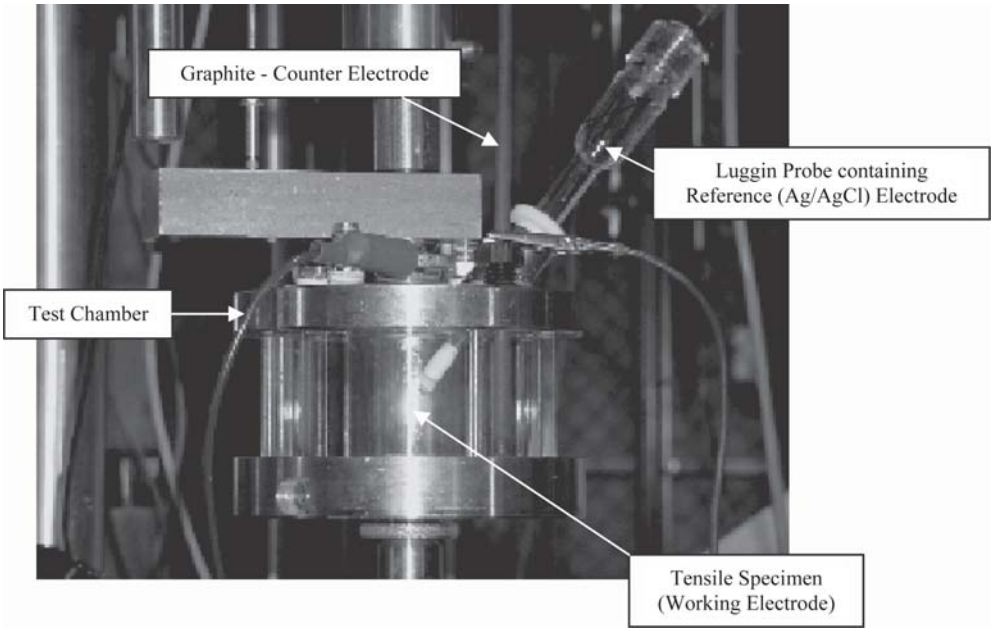

Fig. 3 SSR test setup under controlled potential

3. Experimental Procedures

Prior to the fabrication of the test specimens, the hardness of Alloy EP-823 was measured after both austenitizing and quenching and tempering operations using the Rockwell hardness testing machine in the C scale (R_c). Subsequently, the metallurgical microstructures were determined by optical microscopy in the polished and etched conditions. The ambient temperature tensile properties were then evaluated using a servohydraulic testing machine at a strain rate of 10^{-3} s^{-1} according to the ASTM Designation E 8-04 (Ref 13). The magnitude of the yield strength (YS), ultimate tensile strength (UTS), percent elongation (%El), and percent reduction in area (%RA) was determined from the engineering stress versus strain (s-e) diagram based on duplicate tensile tests performed on this alloy.

The susceptibility of Alloy EP-823 to localized corrosion was determined by the cyclic potentiodynamic polarization (CPP) technique in the acidic solution at 30, 60, and 90 °C. A three-electrode polarization method involving a working electrode (test specimen), a reference electrode (Ag/AgCl), and two counter electrodes (graphite) was used. The potentiostat used in

Table 4 Ambient-temperature tensile properties

Material/heat No.	YS, ksi (MPa)	UTS, ksi (MPa)	%El	%RA
Alloy EP-823/2055	108 (745)	121 (834)	26.02	62.62

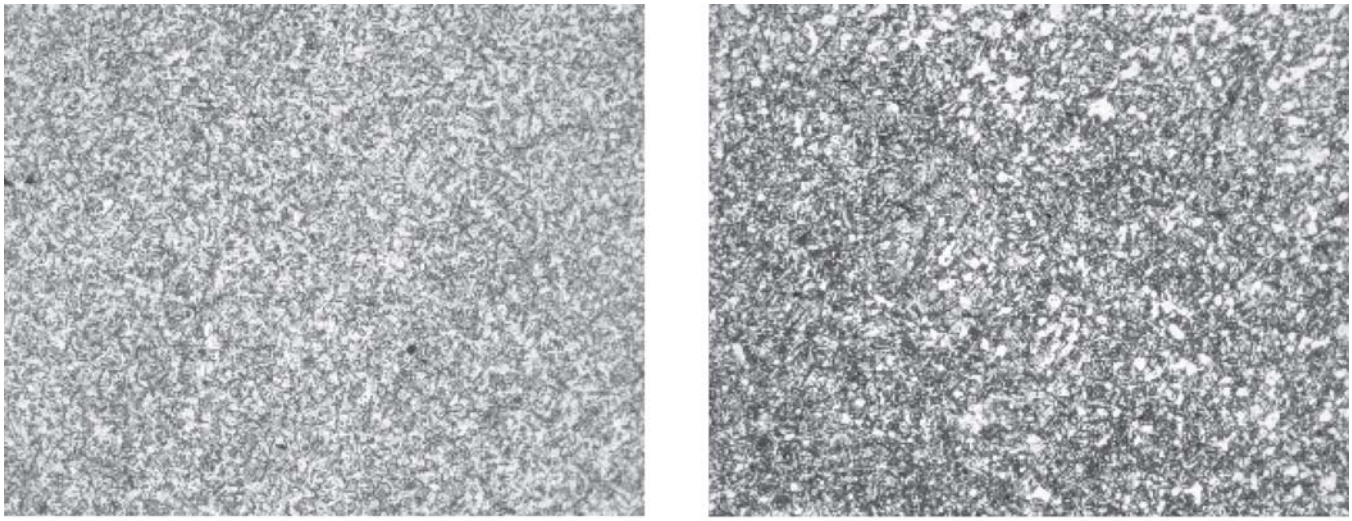

Fig. 4 Optical micrographs of alloy EP-823, etched in Fry's reagent, 200×: (a) austenitized and quenched and (b) quenched and tempered

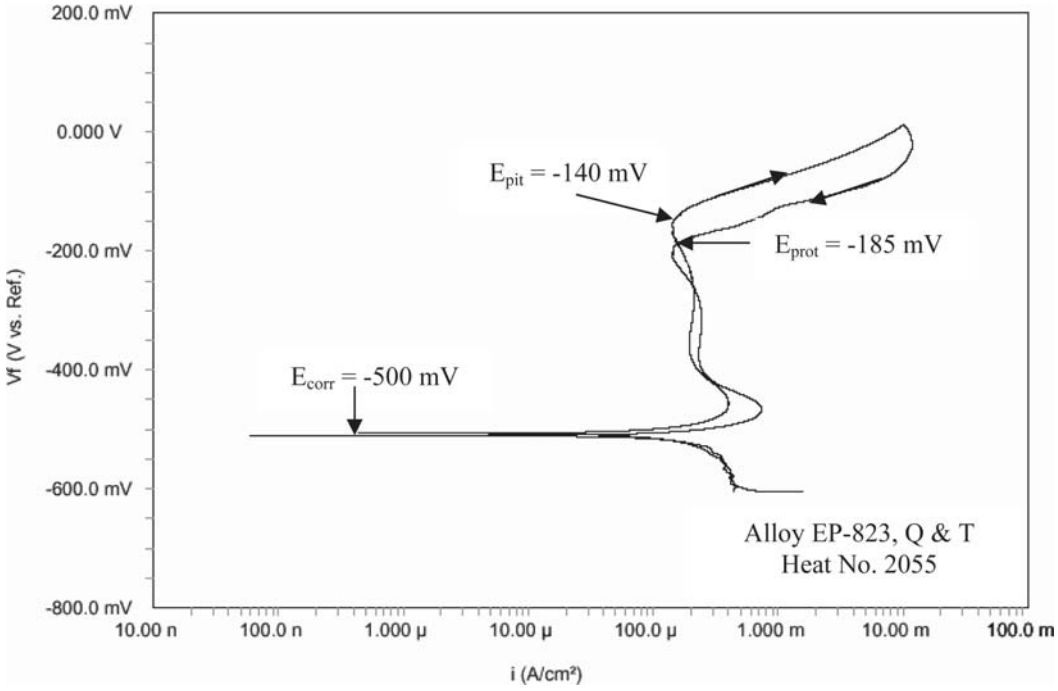

Fig. 5 CPP diagram in 30 °C acidic solution (pH ~ 2.35)

the CPP test was calibrated according to the ASTM Designation G 5-04 (Ref 14) prior to the localized corrosion study.

The cracking behavior of Alloy EP-823 in the acidic solution was evaluated by using the slow-strain-rate (SSR) testing technique at ambient temperature, 60 °C, and 90 °C at a strain rate of 3.3×10^{-6} s^{-1}. The rationale for using this strain rate is given elsewhere (Ref 9-11). The application of this strain rate to the test specimens produced failures that probably would not have occurred at constant load or would have taken a prohibitively longer duration to cause failures in the tested specimens. The experimental setup used in the SSR testing is shown in Fig. 2. During the SSR testing, the load versus dis placement curve, and the engineering stress versus strain (s-e) diagram of Alloy EP-823 were generated. The dimensions (gauge length and gauge diameter) of the test specimens were measured before and after testing. The test specimens were subjected to a continuously changing stress. The cracking tendency was characterized by the %El, %RA, time-to-failure (TTF), and true failure stress (σ_f). The magnitude of σ_f was based on the failure load under a specific environmental condition, and the final cross sectional area of the gage section at failure. Thus, σ_f is different from the engineering failure stress (s_f).

The susceptibility of Alloy EP-823 to HE was evaluated by applying a controlled cathodic potential (E_{cont}) to the test specimens loaded in tension under a SSR condition. This type of potentiostatic polarization is commonly used to evaluate HE in susceptible materials (Ref 9-12). The magnitude of the E_{cont} was based on the corrosion potential (E_{corr}) of Alloy EP-823 determined in a similar environment by the CPP technique. A potential, active (negative) to the E_{corr} value (−1000 mV versus Ag/AgCl) was applied during the SSR testing under potentiostatic control. The cylindrical specimen used in the E_{cont} testing was spot welded with a conductive wire at its top shoulder to apply the desired potential. This wire was coated with a lacquer to prevent its contact with the test solution during straining of the specimen. The experimental setup used in the SSR testing under E_{cont} is illustrated in Fig. 3. The cracking tendency under E_{cont} was also characterized by the %El, %RA, TTF, and σ_f. Comparisons were made among these parameters with and without the E_{cont}.

Metallographic and fractographic evaluations of all broken cylindrical specimens were performed by optical microscopy (OM) and scanning electron microscopy (SEM), respectively. The characteristics of secondary cracks, if any, along the gage section of the tested specimens were evaluated by OM. The extent and morphology of cracking at the primary fracture surface of the tested specimens were determined by SEM.

4. Results and Discussion

4.1 Effect of Heat Treatment on Hardness, Microstructure, and Tensile Properties

The results indicate that the hardness (R_c) of Alloy EP-823 was significantly reduced in the quenched and tempered (Q & T) condition, compared to that in the quenched only condition, as shown in Table 3. The effect of tempering on hardness may be attributed to the homogenization of the metallurgical microstructure and reduction in internal stresses.

An examination of the optical micrographs (Fig. 4) of Alloy EP-823 under different thermal treatment conditions revealed fine-grained tempered-martensitic microstructures. A similar type of microstructure has been reported in quenched and tempered (Q & T) martensitic Types 410 and 420 stainless steels (Ref 15). The ambient temperature tensile properties of Q & T Alloy EP-823 are given in Table 4.

4.2 Results of CPP Testing

The results of CPP testing conducted in the acidic solution at 30 and 90 °C are shown in Fig. 5 and 6, identifying the corrosion potential (E_{corr}), critical pitting potential (E_{pit}), and protection potential (E_{prot}), if any. An examination of these diagrams indicates that the magnitude of E_{corr} at 90 °C was

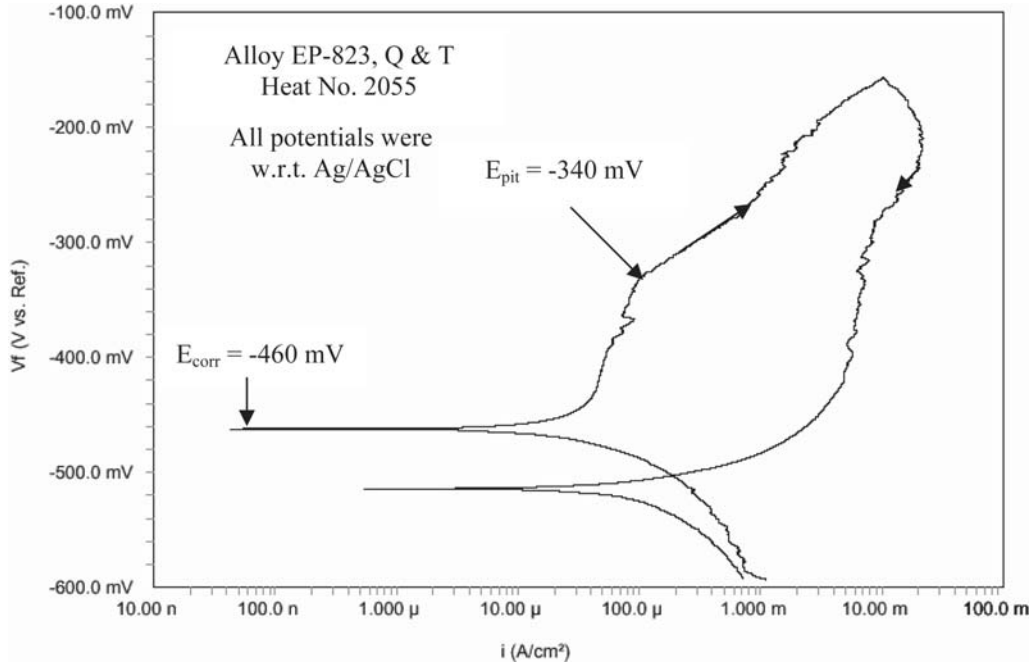

Fig. 6 CPP diagram in 90 °C acidic solution (pH ~ 2.35)

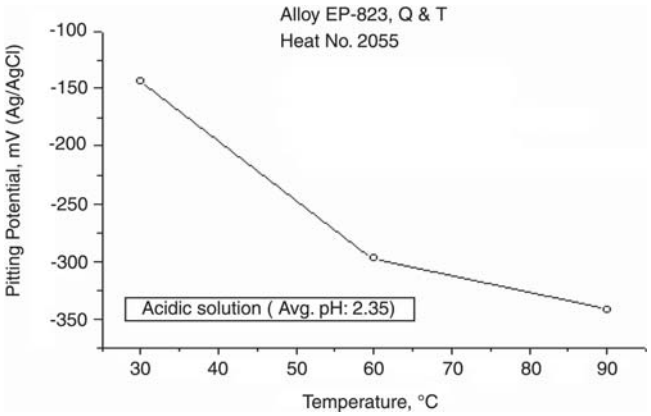

Fig. 7 Effect of temperature on critical pitting potential

slightly more noble (−460 mV, Ag/AgCl), than that at 30 °C (−500 mV, Ag/AgCl). The variation of the average E_{pit} value, determined from the CPP testing, is illustrated in Fig. 7. An evaluation of these data indicates that the magnitude of E_{pit} gradually became more active (negative) with increasing temperature. A similar effect of temperature on E_{pit} has been reported elsewhere (Ref 16).

A comparison of Fig. 5 and 6 also indicates that no protection or repassivation potential (E_{prot}) was observed at 90 °C, possibly caused by the breakdown of the surface film under the combined effect of acidic pH and elevated temperature. The appearances of the polarized specimens in the acidic solution at 30 and 90 °C are illustrated in Fig. 8, showing deeper pits at the elevated temperature. However, the tested specimens showed crevice corrosion at both temperatures.

4.3 Results of SCC Testing with and without E_{cont}

The results of SSR testing of Alloy EP-823 in the acidic solution without E_{cont} are illustrated in Fig. 9, showing s-e diagrams as a function of the testing temperature. This figure also shows an s-e diagram obtained in air for comparison purposes. An examination of these s-e diagrams reveals that the magnitude of the failure strain was reduced with increasing temperature. Obviously, the maximum failure strain was noted in the s-e diagram obtained in air at room temperature (RT). The results of SCC testing performed in a similar environment at 30, 60, and 90 °C under an E_{cont} value of −1000 mV (Ag/AgCl) are shown in Fig. 10. A similar effect of temperature on the cracking susceptibility was observed under E_{cont} once again, showing reduced failure strain at higher testing temperatures.

The data presented in Fig. 9 and 10 are reproduced in Table 5, showing σ_f, %El, %RA, and TTF, with and without E_{cont}. As indicated earlier, the determination of %El, %RA, and σ_f was based on the s-e diagram and the dimensions of the cylindrical specimens before and after testing. An evaluation of these data indicates that the magnitude of all these parameters was reduced under an E_{cont} value of −1000 mV (Ag/AgCl), compared with those obtained without the E_{cont}. However, the extent of reduction of all these parameters was more pronounced at 90 °C, indicating a detrimental effect of higher testing temperature on the cracking susceptibility of Alloy EP-823, with or without the E_{cont}. Comparisons of all four parameters, with and without the E_{cont}, are illustrated in Fig. 11-14, as a function of

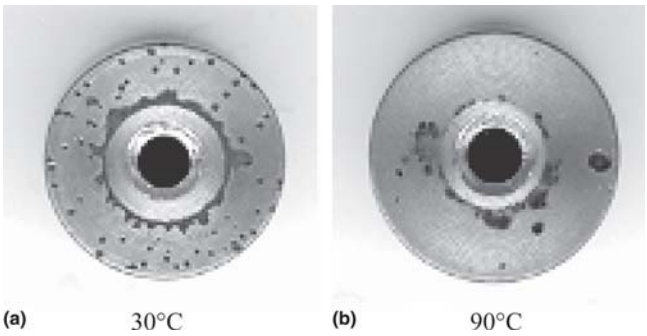

Fig. 8 Appearances of polarized specimens in acidic solution

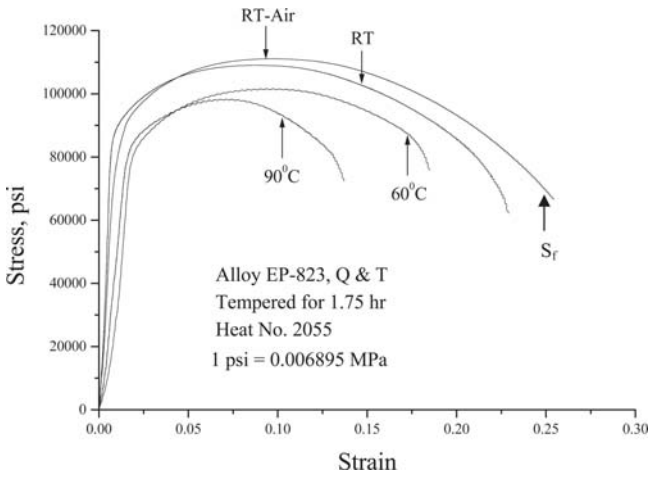

Fig. 9 Stress-strain diagrams in acidic solution (pH ~ 2.35)

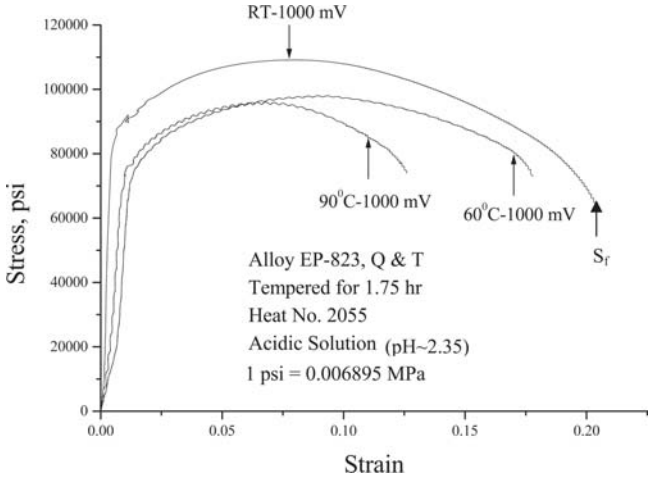

Fig. 10 Stress-strain diagrams under E_{cont}

different testing temperature. The detrimental effects of higher temperature and cathodic potential on the cracking susceptibility are illustrated in these figures. A similar effect of cathodic applied potential on the cracking susceptibility of engineering materials has been reported by other investigators (Ref 9-12, 17-20). However, no attempt has been made to analyze the concentration of hydrogen resulting from the cathodic applied potential.

The initiation of cracking in structural materials in the pres-

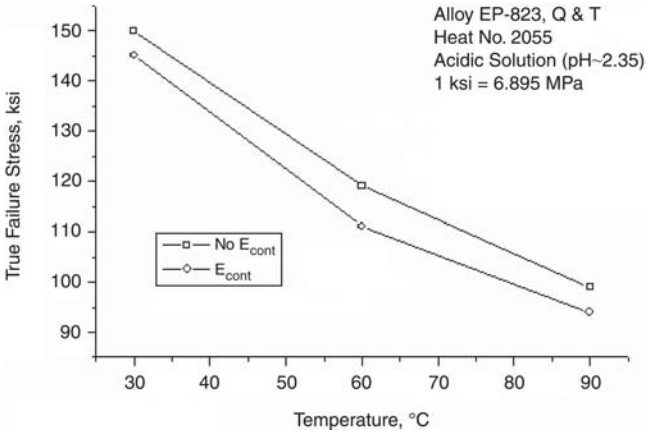

Fig. 11 Effect of temperature on true failure stress (σ_f)

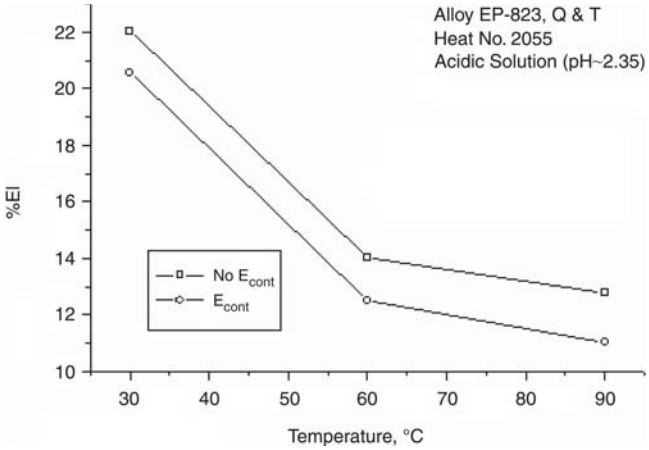

Fig. 13 Effect of temperature on %El

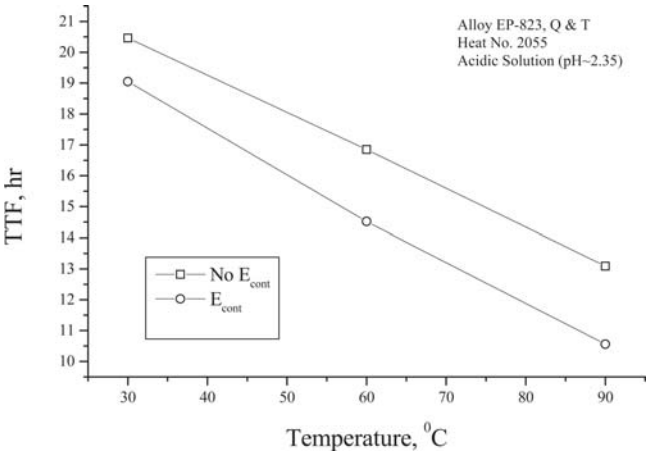

Fig. 12 Effect of temperature on TTF

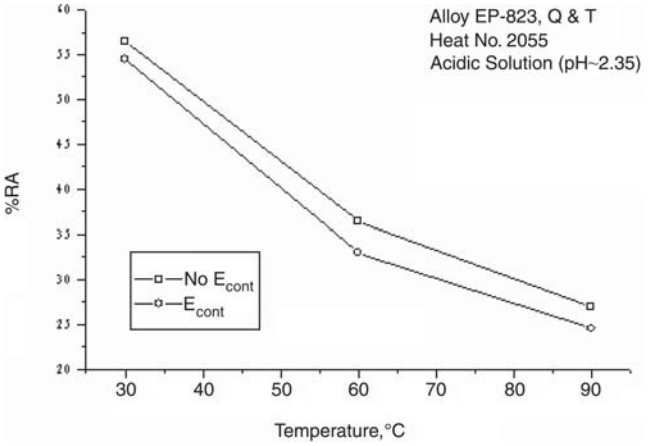

Fig. 14 Effect of temperature on %RA

Table 5 Comparisons of SSR test results with and without E_{cont}

Environment	Temperature, °C	E_{cont} Ag/AgCl, mV	σ_p, ksi (MPa)	%El	%RA	TTF, h
Air	Ambient	None	174 (1200	24.35	60.67	23.15
Acidic solution	Ambient	None	150 (1034)	22.05	56.50	20.46
(average pH ≈ 2.35)	Ambient	−1000	145 (1000)	20.55	54.50	19.05
	60	None	119 (821)	17.50	36.50	16.85
	60	−1000	111 (765)	17.00	33.00	14.52
	90	None	99 (683)	12.80	27.00	13.09
	90	−1000	94 (648)	11.75	24.50	10.56

ence of chloride solutions has been attributed (Ref 21, 22) to planar slip and the formation of wide slip steps that may rupture the protective surface-oxide films. Unless rapid repassivation of these surface films occurs, an active trench may be formed due to the localized anodic dissolution at the metal surface. This active trench, if sufficiently localized, can eventually cause the stress corrosion crack growth.

Two theories have been proposed (Ref 21, 22) to account for SCC propagation in susceptible materials. One theory is based on anodic dissolution of metal surface at highly localized areas of stress concentration such as crack tip, which can aid in crack propagation into the metal matrix by the applied tensile stress. The alternate mechanism is focused on the HE phenomenon that may account for the cracking of Alloy EP-823 studied in this program. This mechanism postulates that hydrogen absorption can result from localized anodic dissolution in a hydrogen-containing aqueous solution, and the formation of film-free surfaces within the advancing crack. Absorbed hydrogen may then migrate and concentrate near the crack tip due to the existing tensile stress gradients. Localized HE of the metal ahead of the crack can subsequently aid in continued crack propagation.

4.4 Results of Microscopic Evaluations

The evaluations of the primary fracture surface of the cylindrical specimens tested under the SSR condition by SEM showed combined ductile and brittle failures, irrespective of

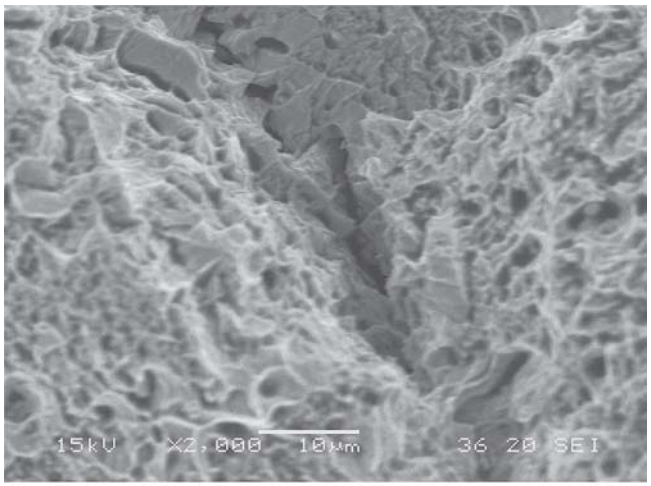

(a)

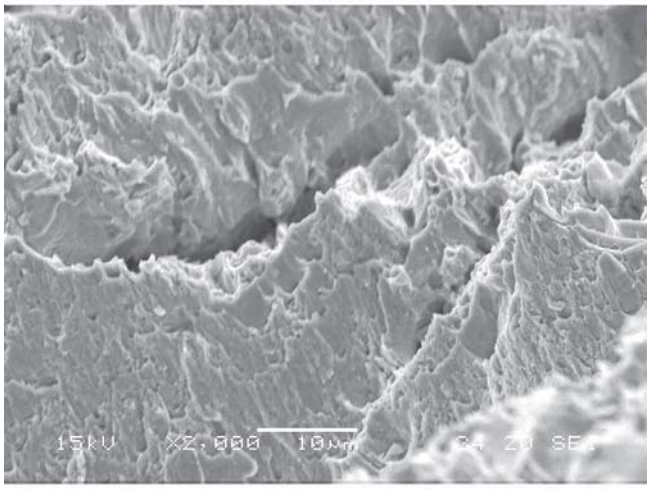

(b)

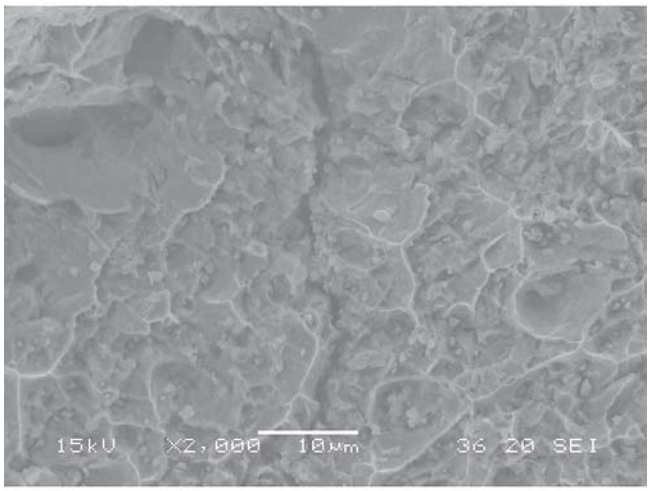

(c)

Fig. 15 SEM micrographs of alloy EP-823 (no E_{cont}): (a) 30 °C, 2000×, (b) 60 °C, 2000×, and (c) 90 °C, 2000×

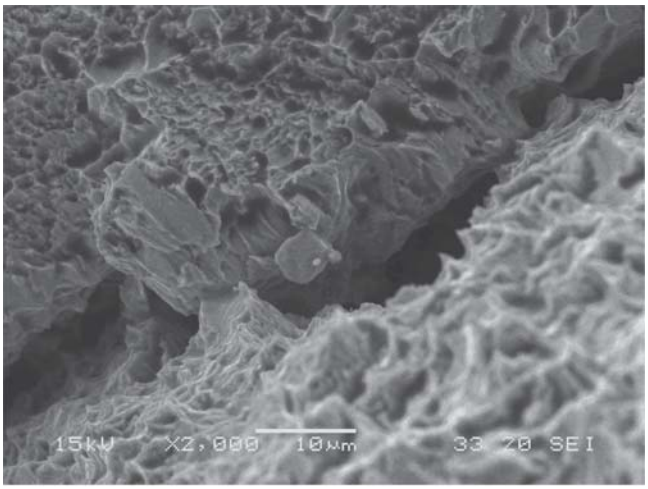

(a)

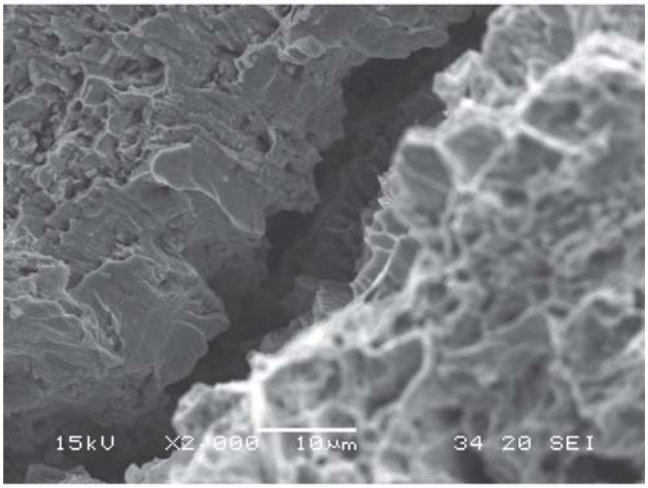

(b)

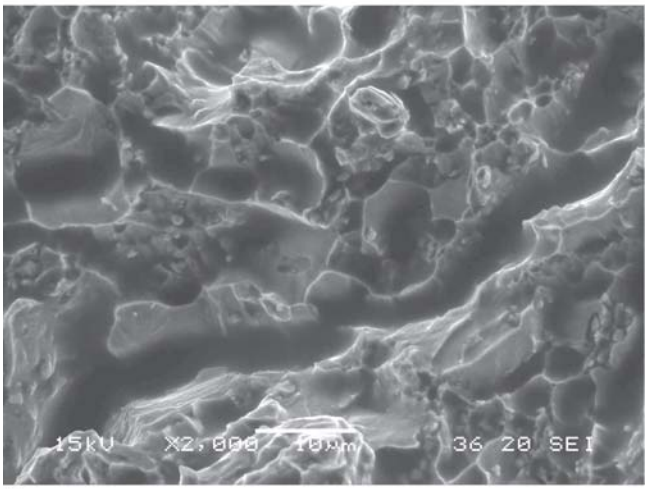

(c)

Fig. 16 SEM micrographs of alloy EP-823 (with E_{cont}): (a) 30 °C, 2000×, (b) 60 °C, 2000×, (c) 90 °C, 2000×

the application of E_{cont}, as shown in Fig. 15 and 16. The ductile failures were characterized by the presence of dimpled microstructure. Simultaneously, transgranular cracks caused by cleavage failures were observed in these SEM micrographs. The extent of brittleness was, however, more pronounced in specimens tested under E_{cont} at higher temperatures, as noted by the wider transgranular cracks. Branched secondary cracks were also observed in all cylindrical specimens, with and with-

Fig. 17 Optical micrograph of secondary cracks (no E_{cont}), etched in Fry's reagent, 200×

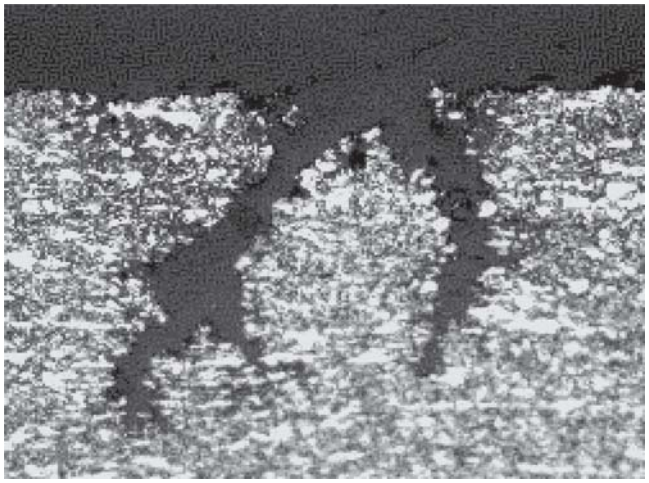

Fig. 18 Optical micrograph of secondary cracks (with E_{cont}), etched in Fry's reagent, 200×

out the application of E_{cont}, as shown by optical micrographs in Fig. 17 and 18.

5. Summary and Conclusions

The susceptibility of Alloy EP-823 to localized corrosion, SCC, and HE has been evaluated in an acidic solution at 30, 60, and 90 °C. The localized corrosion behavior was studied by the CPP technique. The cracking susceptibility was evaluated by the SSR method, with and without the E_{cont}. Metallographic and fractographic evaluations were performed by optical microscopy and SEM, respectively. The significant conclusions are given below.

- All polarized specimens exhibited pits and crevices, showing deeper pits at elevated temperatures. The critical pitting potential became more active at higher temperatures.
- The magnitude of σ_f, TTF, %El, and %RA was gradually reduced with increasing temperature. The extent of reduction of these parameters was more pronounced under an E_{cont} value of −1000 mV (Ag/AgCl).
- A combination of ductile and transgranular brittle failures was observed by SEM on the primary fracture surface of the tested specimens. The extent of failure, in terms of the width of the transgranular crack, was more severe under E_{cont}.
- Branched secondary cracks were observed along the gage section of the tested cylindrical specimens.

Acknowledgment

This work was funded by the UNLV Transmutation Research Program (TRP) administered by the Harry Reid Center for Environmental Studies under the United States Department of Energy Grant No. DE-FG04-2001AL67358.

References

1. P. Jung, C. Liu, and J. Chen, Retention of Implanted Hydrogen and Helium in Martensitic Stainless Steels and Their Effects on Mechanical Properties, *J. Nucl. Mater.,* 2001, **296**(1-3), p 165-173
2. H. Rauh and H. Ullmaier, Hydrogen Concentrations Near Cracks in Target Materials for High-Power Spallation Neutron Sources, *J. Nucl. Mater.,* 2001, **295**(1), p 109-120
3. V.S. Khabarov, V.D. Dmitriev, A.M. Dvoriashin, V.V. Romaneev, and E.A. Medvedeva, Mechanical Properties and Microstructure of Neutron-Irradiated Ferritic-Martensitic Steel, Used as Wrapper Material for the BN-350 and BN-600 Fast Reactor, *Proc. Int. Conf. Fast Reactor Core and Fuel Structural Behavior,* Inverness, June 4-6, 1990, (Inverness, Scotland), p 263-267
4. A.G. Ioltukhovski, A.I. Blokhin, N.I. Budylkin, V.M. Chernov, M.V. Leont'eva-Smirnova, E.G. Mironova, E.A. Medvedeva, M.I. Solonin, S.I. Porollo, and L.P. Zavyalsky, Material Science and Manufacturing of Heat-Resistant Reduced Activation Ferritic-Martensitic Steels for Fusion, *J. Nucl. Mater.,* 2000, **283-287,** p 652-656
5. S.I. Porollo, Yu.V. Konobeev, A.M. Dvoriashin, N.I. Budylkin, E.G. Mironova, M.V. Leontyeva-Smirnova, A.G. Loltukhovsky, A.A. Boinchvar, and F. A. Garner, Irradiation Creep and Meinchanical Properties of Two Ferritic/Martensitic Steels Irradiated in the BN-350 Fast Reactor, Oak Ridge National Laboratory, 2002, p 106-114
6. A.K. Roy, M.K. Hossain, R. Prabhakaran, and S. Sama, Environment-Assisted Cracking of Structural Materials Under Different Loading Conditions, *Corrosion,* 2005, **61**(4), p 364-370
7. H. Satoh, T. Fukuzuka, K. Shimogori, and H. Tanabe, Hydrogen Pickup by Titanium Held Cathodic in Seawater, *2nd International Congress on Hydrogen in Metals,* Paper 6A1, presented June 1977 (Paris, France)
8. R.W. Schutz and J.S. Grauman, Determination of Cathodic Potential Limits for Prevention of Titanium Tube Hydride Embrittlement in Salt Water, Paper 110, presented at *NACE Corrosion 1989,* (New Orleans, LA), NACE International, 1989
9. A.K. Roy and M.K. Spragge, Effect of Controlled Potential on SCC of Nuclear Waste Package Container Materials, Paper 00188, presented at *NACE Corrosion 2000* (Orlando, FL), 2000
10. A.K. Roy, J.C. Estill, S.R. Gordan, and L.F. Logoteta, Stress Corrosion Cracking of Ni-Base and Ti Alloys Under Controlled Potential, Paper ICONE-7048, presented at *7th International Conference on Nuclear Engineering* (Tokyo, Japan), April 19-23, 1999
11. A.K. Roy, M.K. Spragge, D.L. Fleming, and B.Y. Lum, Cracking of Titanium Alloys under Cathodic Applied Electrochemical Potential, *Micron,* 2001, **32**(2), p 211-218
12. I. Azkarate, A. Pelayo, and L. Victori, Hydrogen Assisted Stress Cracking of Titanium Alloys in Aqueous Chloride Environments, *Progress in the Understanding and Prevention of Corrosion,* Vol. 2, Spain, 1993, p 1573-1580
13. ASTM Designation, E8-04, "Standard Test Methods for Tension Testing of Metallic Materials," American Society for Testing and Materials (ASTM) International, 2004
14. ASTM Designation, G5-04, "Standard Reference Method for Making Potentiostatic and Potentiodynamic Anodic Polarization Measurements," American Society for Testing and Materials (ASTM) International, 2004
15. Metallography and Microstructures, *ASM Handbook,* Vol 9, ASM International, 2000, p 292
16. A.K. Roy, D.L. Fleming, and B.Y. Lum, Effect of Environmental Variables on Localized Corrosion of High-Performance Container Ma-

terials, *Proc. ICONE5,* May, 1997 (Nice, France) ASME/SFEN/JSME, p 1-11
17. G.P. Tiwari, A. Bose, J.K. Chakravartty, S.L. Wadekar, M.K. Totlani, R.N. Arya, and R.K. Fotedar, Study of Internal Hydrogen Embrittlement of Steels, *Mater. Sci. Eng. A,* 2000, **286**(2), p 269-281
18. A.R. Troiano, The Role of Hydrogen and other Interstitials in the Mechanical Behavior of Metals, *Trans. Am. Soc. Metals,* 1960, **52**(1), p 54-80
19. R.A. Oriani, Hydrogen Embrittlement of Steels, *Ann. Rev. Mater. Sci,* 1978, **8,** p 327-357
20. J.P. Hirth, Effects of Hydrogen on the Properties of Iron and Steel, *Metall. Trans.,* 1980, **11A,** p 861-889
21. J. Brettle, Stress Corrosion of Titanium and Its Alloys in Aqueous Chloride Environments, *Metall. Mater.,* 1972, **6**(10), p 442-451
22. R.J.H. Wanhill, Aqueous Stress Corrosion in Titanium Alloys, *Brit. Corros. J,* 1975, **10**(2), p 69-78